Intersite Magnetic Signals from Lightning

Matthew Ball
Robert Schofield
Raymond Frey

November 10, 2020

Abstract

Comparison of LEMI Omicron triggers with Vaisala's GLD360 data set is used to establish the detection of lighting by the LEMIs, primarily in North America. Coincident millisecond scale transients in LHO and LLO LEMI magnetometer signals occur at a rate of about 1000-2000 events per hour and reach up to at least 900 Hz. Roughly 50% of the LEMI coincidences are also coincident with Vaisala-identified lightning strokes. Of the Vaisala-identified strokes in North America, 1.6% are coincident with LHO-LLO LEMI coincidences. For Vaisala-identified lightning strokes outside North America, there are almost no LEMI coincidences. Coincident Vaisala-identified strokes slightly favor ground-to-cloud transmission. Coincident LEMI signals tend to favor higher frequencies. These lightning signals are consistent with being responsible for the observed high-frequency magnetic coherence between LHO and LLO. Including magnetometer signals from Virgo highlights higher current lightning at higher SNR. Three-site coincidences still emphasize lightning signals in North America, but also make clear regions of sensitivity in South America and the Northern Mediterranean. Comparing coincidences with normal lightning to signals coincident with observed gigantic jets suggest that these jets do not pose any more of a problem than the strongest lightning signals.

1 Introduction

The extreme sensitivity of the LIGO detectors makes it necessary to understand all potential sources of non-gravitational wave signals. Signals coincident between both LIGO Hanford and LIGO Livingston are especially concerning. Possible sources of coincident signals include Schumann resonances, lightning, and gigantic jets. Schumann resonances have been explored in detail before [1], but the effects of lightning and gigantic jets have not been fully investigated.

The PEM network includes a multitude of environmental sensors, including accelerometers, seismometers, microphones, and magnetometers. With regards to detecting magnetic signals, the array includes fluxgate magnetometers (Bartington Mag-O3) inside the facilities, but it also includes more sensitive LEMI magnetometers in the vaults located roughly a kilometer from the nearest buildings (and 100-200 m from the beam tubes). Being far away from regular anthropogenic sources of noise, these magnetometers are more suitable for examining stochastic noise sources than the Bartingtons which are susceptible to building-specific sources.

Studies performed by the Stochastic working group have indicated magnetic coherence beyond the known Schumann resonances between the two LIGO sites, which could be problematic for stochastic gravitational wave searches as the detectors' sensitivity improve [5]. A magnetic signal capable of generating a false gravitational wave signal coincident between the two LIGO sites would be clearly observed by the sensitive LEMI magnetometers at each site. By collecting magnetic signals coincident between the two sites, we should have a set of signals which can be evaluated for potential contributions to gravitational wave candidate events.

In this study, we compare coincident magnetic signals with an external data set of known lightning strokes and use this to estimate the range of sensitivity to lightning and the potential rate of coincident signals. We also determine some properties of the signals that are associated with lightning. With known gigantic jets in the data as well, we can identify characteristic details of their waveform that separate them from ordinary lightning.

LIGO-T2000634-v1

2 Methods

2.1 Coincident LEMI Signals: Anectodal motivation

On September 24, 2019, a gigantic jet was observed over Tropical Storm Karen in the Caribbean Sea [7]. Examining the LEMI magnetometers at the time of this jet revealed broadband signals at both LIGO Hanford and LIGO Livingston roughly 0.02 s apart. These signals were only observed in the X and Y axes of these magnetometers, not Z (here, X and Y axes align with X and Y arms of the interferometers).

Figure 1 shows spectrograms of the four magnetometer axes studied during this gigantic jet. The signal peaks at lower (sub-60Hz) frequencies, placing it right in the center of the sensitivity band. Figure 2 shows filtered timeseries for this jet. The signals were lowpassed at 55Hz with a notch filter at 60Hz. This event suggested that only the X and Y axes of the magnetometers would regularly pick up the signals from lightning, so the Z axis was ignored for signal detection.

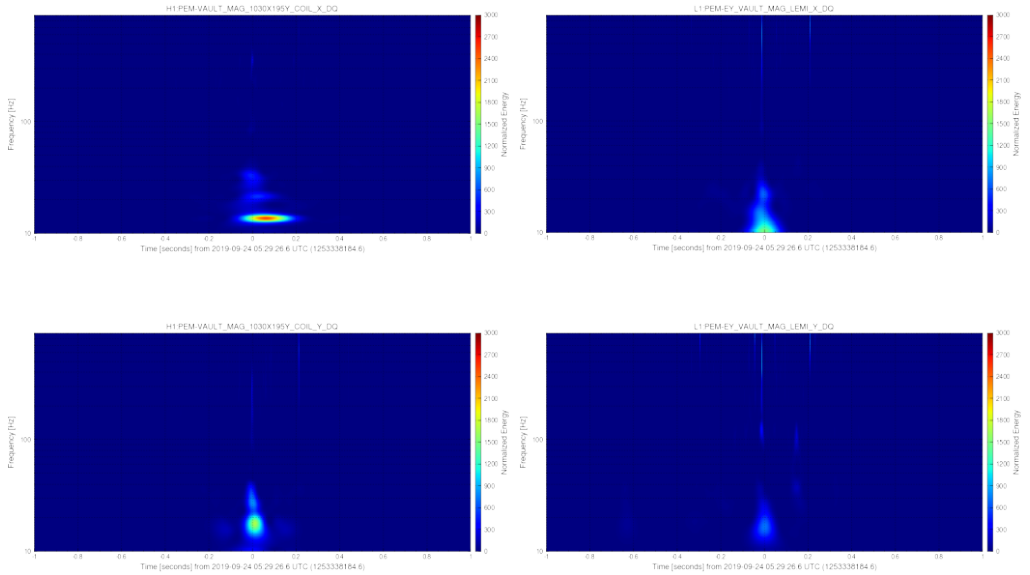

Figure 1: Spectrograms of LEMI signals due to gigantic jet on September 24, 2019. Left column shows spectrograms from Hanford and right column shows spectrograms from Livingston. Top row aligns with respective X arms, and bottom row aligns with respective Y arms. Peak frequencies are below 100 Hz and clearly visible at both sites.

2.2 LEMI Triggers from Omicron

LEMI magnetometers at both LIGO Hanford and LIGO Livingston were examined for excess noise during the week of September 23, 2019. The X and Y axes of these magnetometers were analyzed using the Omicron tool which looks for excess energy via sine-Gaussian fits. Omicron performed 64 second PSDs with 4 second overlaps in the frequency range 10-900 Hz (limited by a Q-scan's upper limit of 63% of the Nyquist frequency) for a Q range between 4 and 64. A minimum SNR of 5.5 was required, and triggers were clustered in time. Omicron returns the start and end time of each trigger cluster with the minimum and maximum frequency the trigger occupies. It also returns the time and frequency of the maximum energy (deviation from the average background) of the trigger which were recorded as "peak times" and "peak frequencies" [8].

To get a comprehensive list of coincident LEMI signals, triggers whose peak times were within 0.0005 s of another trigger from the orthogonal channel at the same site, and within 0.022 s of at least one trigger from a channel at the other site were collected (thus requiring at least 3 of these 4 magnetometer channels to see the signal). The time that each trigger was detected at each site was recorded. These threshold values were chosen from the anecdotal evidence from the September gigantic jet described earlier.

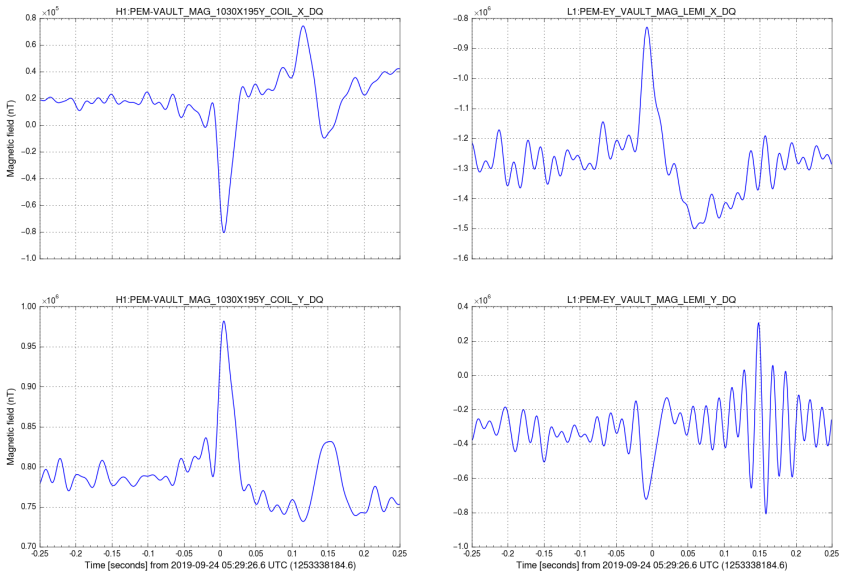

Figure 2: Time series of LEMI magnetometers at both LIGO sites at the time of the gigantic jet near Puerto Rico on September 24, 2019.

2.3 Vaisala Global Lightning Database

These coincident LEMI signal lists were compared to the Vaisala GLD360 data set [11] for the same time period. Worldwide lightning strokes with 10 km spatial and 1 μs temporal resolution were collected from VLF radio signals. A broad network of GPS-synchronized sensors used matched waveforms to estimate the location of a stroke as well as an estimate of the peak current. The current was recorded to the nearest kA, with polarity determined by the direction of the electric field - a negative current is assigned for an electric field pointing toward the Earth [11]. The Vaisala network claims an 80% detection efficiency in identifying cloud-to-ground strokes in the northern hemisphere and between 10% and 80% detection efficiency in the southern hemisphere [2, 6].

2.4 NASA Geostationary Lightning Mapper

We also were interested in how our data set compared with the publicly available GLM data set from NASA [4]. This data set is collected by the NASA GOES (Geostationary Operational Environmental Satellite) project. The particular data examined here was collected while the project was in the GOES-East configuration. There is a non-trivial time offset to the GLM data that is described in Appendix A.

The GLM uses a camera to image the Earth, recording flashes of light on a pixel-by-pixel basis. These individual pixels (referred to as "events") are then clustered into "groups" by proximity within the same frame. These groups are then clustered in time into "flashes". All groups in a flash occur within a time span of no more than 330 ms and within a physical range of no more than 16.5 km. To prevent the camera registering light from non-lightning sources (eg. sunlight reflection), the data is all filtered to the range 776.87 - 777.87 nm to focus on the first ionized oxygen line at 777.4 nm [9].

3 Lightning

3.1 Establishing Coincident Signals with GLD360

The distance from each stroke to each site was computed and with it, the required travel time for a signal traveling at the speed of light. The difference in time between each Vaisala-identified stroke and each LEMI signal was then computed for each site. If the difference between this time

difference and the required light travel time was less than 0.005 s for both sites, the LEMI signal and this stroke were associated as matching.

The GLD data was clustered into groups via kmeans clustering and a timeslide analysis was performed on each cluster. By varying an additional time offset to the GLD data and examining the number of coincident strokes, the validity of coincident strokes could be established. If a timeslide had no clear spike above background (Figure 3), the cluster would be ignored for coincidence checks. If the timeslide did have a large spike above background (Figure 4), that cluster would be identified as having a higher probability that strokes coincident with LEMI signals were real. After each cluster with a timeslide spike was identified, the strokes in them that were coincident with LEMI signals were collected.

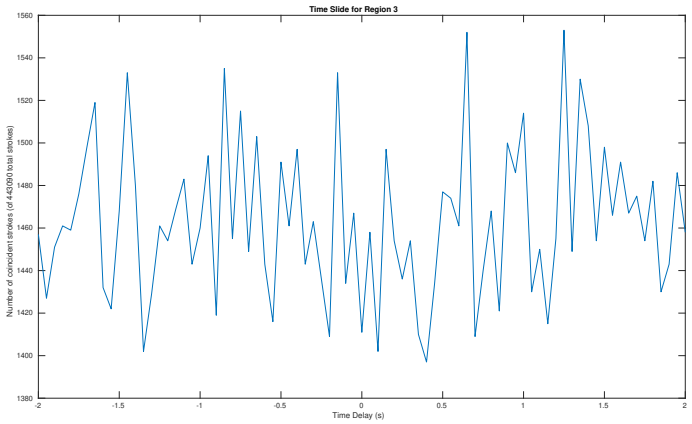

Figure 3: GLD timeslide with no spike for a cluster in central Africa. Since there was no spike, all Vaisala-identified strokes in this cluster were rejected as possible signal sources.

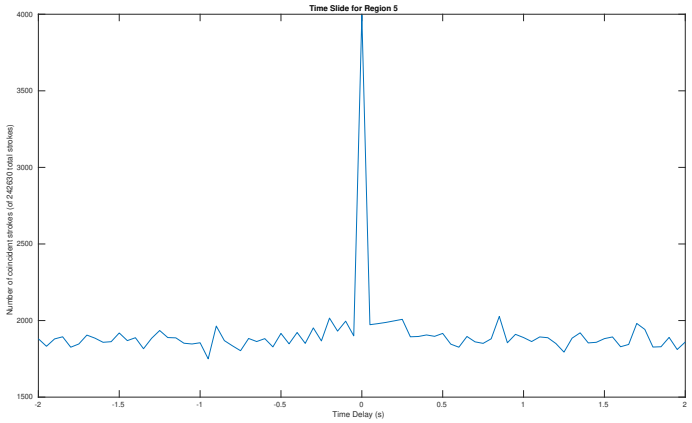

Figure 4: Timeslide with a large spike for a cluster in the central United States. With a spike this large, Vaisala-identified strokes coincident with LEMI signals at 0 offset in the slide were recorded as possible signal sources.

An example of a particularly loud LEMI signal that matched a Vaisala-identified stroke in the aforementioned criteria is shown in Figure 5. This particular signal peaks at higher frequencies (several hundred Hz). This is typical for high-SNR signals that matched Vaisala-identified strokes.

Using this clustered timeslide approach, we find that of the 314928 Omicron triggers coincident between sites, 158232 are coincident with Vaisala-identified strokes (50.2%). Of the 45007030 worldwide Vaisala-identified strokes, 158232 were matched to coincident Omicron triggers (0.38%). When only counting strokes in the North America region, we count 9825560 strokes with 157996 matching to coincident Omicron triggers (1.61%). All histograms presented below are normalized separately for matched and unmatched to the worldwide counts here.

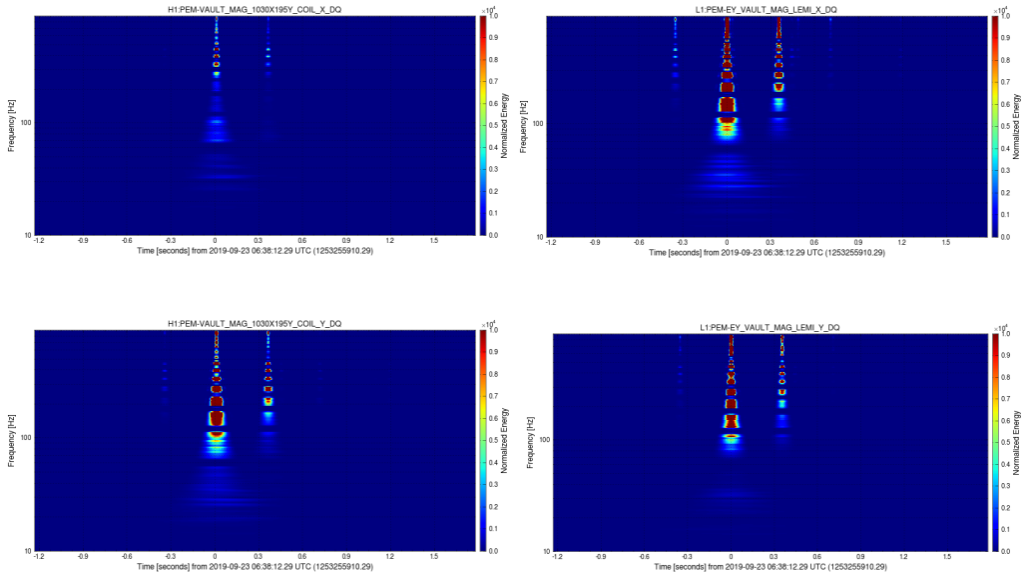

Figure 5: Spectrograms of a particularly loud trigger that was matched to a Vaisala stroke. Left column shows spectrograms from Hanford and right column shows spectrograms from Livingston. Top row aligns with respective X arms, and bottom row aligns with respective Y arms. This stroke-matched signal peaks at hundreds of Hz and appears to reach nearly 1kHz.

3.2 Properties of Detected Strokes

3.2.1 Region of Sensitivity

Figure 6 shows the locations of GLD360 strokes matched to coincident LEMI signals as described earlier, highlighting where lightning was most likely detected. This suggests that lightning in the continental United States, Central America, the Gulf of Mexico, and parts of northern South America are where strokes would most likely cause coincident magnetic signals in the LEMIs. The maximum distance from a matched stroke to each site was 7277 km for Livingston and 8629 km for Hanford. This does not rule out the possibility of LEMI sensitivity to loud signals at greater distances. Lone gigantic jets or strong lightning strokes that cause signals in LEMIs but are not in a cluster with a large timeslide spike would be ignored.

3.2.2 Parameters of Matched Vaisala-Identified Strokes and LEMI Signals

The GLD360 dataset also includes estimates of peak current for each stroke. Figure 7 shows the distribution of currents for coincident strokes compared to non-coincident strokes. While both distributions resemble Poisson distributions in both positive and negative currents, the matched strokes have a far less symmetric distribution about zero. This suggests that the LEMI magnetometers are more adept at picking up signals from strokes with a negative current (electric field pointing toward Earth).

Only one documented gigantic jet fell within the week of September 23 that we had GLD360 data for, the current of this signal fell near the center of the current distribution. Since gigantic jets are predicted to have far greater current magnitudes than this, this detection is most likely from the associated cloud to ground stroke and not from the jet itself.

3.3 Matching Omicron Trigger Parameters

As for the LEMI signals that matched these strokes, their frequency distribution is shown in figure 8 and their SNR distribution is shown in figure 9. The peak frequencies at both sites tend toward higher frequencies for matched signals. Likewise, higher SNR signals are slightly favored over lower SNR signals.

Some of the loudest signals can look nearly identical between sites. Look back at figure 5 which shows spectrograms from a particularly loud LEMI signal that was matched to a Vaisala stroke.

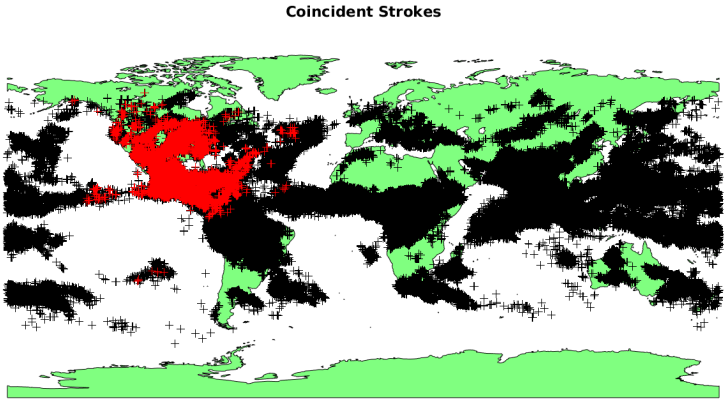

Figure 6: Worldwide lightning strokes from week of September 23, 2019. Red marks are Vaisala-identified strokes in clusters with a sufficiently large spike in a timeslide with coincident magnetometer signals. Coincidence with LEMI signals suggest the highest sensitivity around North America.

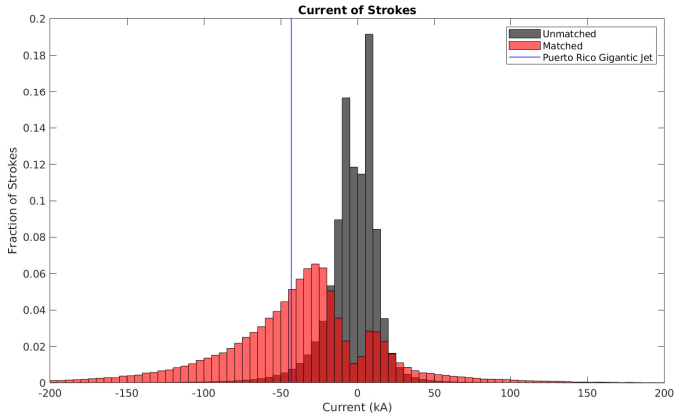

Figure 7: Current distribution for all Vaisala-identified strokes during the week of September 23. Red histogram includes the current distribution of all Vaisala-identified strokes that matched with LEMI signals at both sites. Grey histogram includes all other strokes from the week. Vertical line corresponds to stroke lining up with September 24, 2019 gigantic jet near Puerto Rico. Distributions are normalized to each population.

This particular signal appears as very broadband, stretching far above the frequencies associated with Schumann resonances.

3.4 Inter-site LEMI Coherence

Due to the high-frequency tendency of the LEMI triggers that match Vaisala-identified strokes (Figure 8), we expect to see this manifest in high frequency coherence that exceeds what would be expected for purely Gaussian noise. Figure 10 shows the coherence between 2000 triggers coincident between both sites seen in the LEMI X-axis and coincident with Vaisala-identified strokes. The triggers were stitched together into about two hours of fake data along with two hours of Gaussian noise to represent the diurnal variation in Figure 12. An additional 8000 random signals were injected to simulate non-coincident transients at the rate observed. The horizontal black line represents coherence between two Gaussian noise signals of equivalent length to the simulated data.

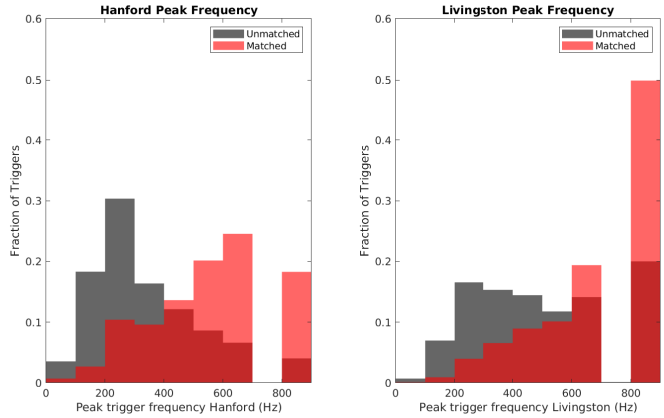

Figure 8: Peak frequency of matched and unmatched Omicron triggers. The same triggers are shown in both plots, but the frequency values recorded at Hanford and Livingston differed. Triggers matched to Vaisala-identified strokes tend to favor higher frequencies than unmatched triggers. Distributions are normalized to each population.

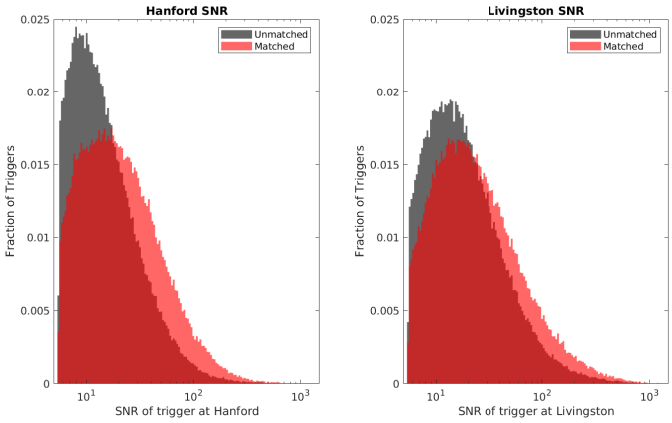

Figure 9: SNR of matched (red) and unmatched (gray) Omicron triggers. The same triggers are shown in both plots, but the SNR values recorded at Hanford and Livingston differed. Notice that higher SNR triggers are slightly favored to be matched to a stroke than lower SNR triggers. Distributions are normalized to each population.

The stochastic group computes Gaussian coherence as 1 over the number of segments (where a segment is 10 seconds). In this manner, the Gaussian coherence background would be much higher, at around 8×10^{-4}. This simulated coherence resembles what the stochastic group observed for magnetic coherence during LIGO's second observing run [5] suggesting that these lightning signals may have been the driving factor for the high frequency coherence observed.

3.5 Coincident Magnetic Signal Rate

We can also look at the rate of these coincident LEMI signals to estimate how frequently we could expect coherent false signals between the sites. Figure 11 shows the rate of coincident LEMI signals that match Vaisala strokes as well as a stroke rate for the region where all coincident strokes were recorded. Coincident LEMI signals were binned by bandwidth which showed that the most broadband signals occur at the highest and most diurnal rate. The strokes used in this stroke rate were restricted by estimated peak current of each stroke divided by the average distance of the stroke to the two LIGO sites. Restricting this value to be outside the range (-0.02 A/m, +0.04 A/m) gives a stroke rate similar to the LEMI trigger rate. The diurnal variation is due to diurnal variations in the ionosphere conductivity that alter how extremely low frequency (ELF) signals can propagate along it. Maximal energy transfer of the ELF signals over great distances

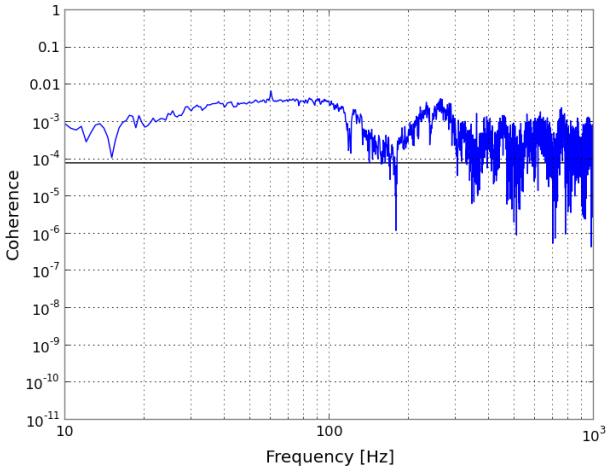

Figure 10: Coherence between 2000 coincident triggers seen in LEMI X-axis channels at each site with two hours of Gaussian noise. An additional 8000 random signals were injected into this to simulate non-coincident transients. The black line represents coherence between two Gaussian noise signals of equivalent length to the simulated data. The equivalent Gaussian coherence background as computed by the stochastic group would be around 8×10^{-4}.

occurs during local night, which coincides with the peaks in the coincident LEMI signal rate [13]. The asymmetric cutoff values that were chosen highlight the preference towards negative currents which translates to a preference towards ground-to-cloud strokes (over cloud-to-ground). These bounds are likely due to an asymmetry between the physical duration of cloud-to-ground (denoted by positive current) and ground-to-cloud strokes (denoted by negative current). Ground-to-cloud strokes on average last longer so they should be more efficiently detected [10].

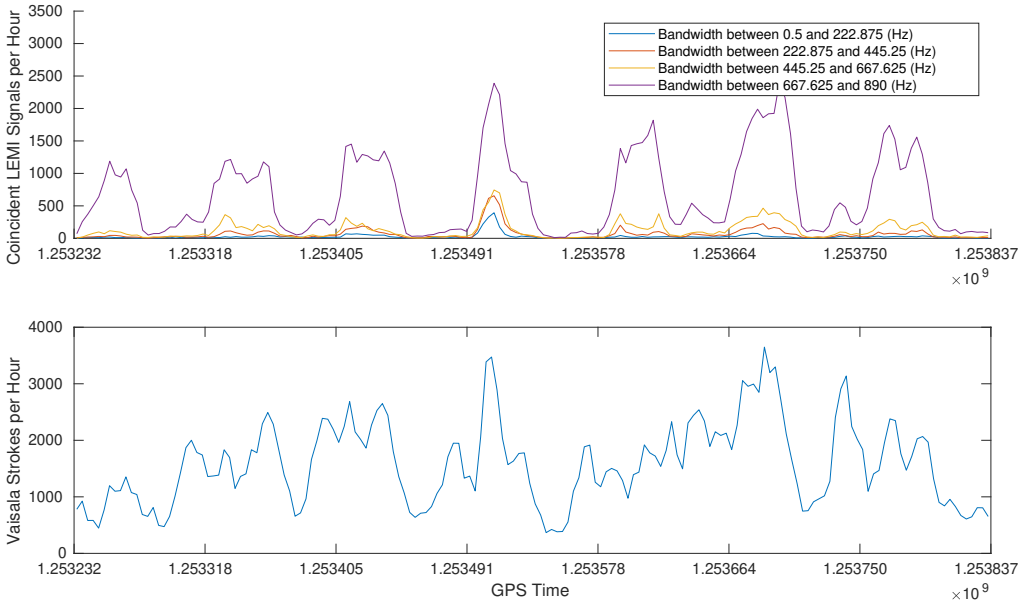

Figure 11: Above: Rate of coincident LEMI signals for one week. X-axis marks represent 1 day increments. A highly diurnal signal rate is primarily associated with the most broadband signals. The bandwidth of these broadband signals is limited by the maximum frequency Omicron could Below: Stroke rate of lightning from Vaisala in North America. Strokes used here are all strokes in the region where strokes coincident with LEMI signals were detected. Restricting the current-over-distance metric as described earlier gives a Vaisala-identified stroke rate similar to the LEMI trigger rate with many similar time-dependent features.

Figure 12 shows this same data divided up into LEMI signals coincident with Vaisala-identified strokes in the area between the sites and LEMI signals coincident with Vaisala-identified strokes further away. Shaded regions mark local night at the halfway point between sites. LEMI signals coincident with Vaisala-identified strokes between the sites have some variation between day and night but mostly line up with the filtered Vaisala-identified stroke rate. However, LEMI signals coincident with Vaisala-identified strokes further from the sites have a far more striking diurnal variation that is not as clearly represented in the Vaisala-identified stroke rate. This behavior is potentially due to variations in the conductivity of the ionosphere due to solar radiation that limits how far these sub-kilohertz signals can effectively travel [13]. Vaisala utilizes two separate banks of waveforms for day and night to account for diurnal differences in how the signals propagate [12]. Unfiltered Vaisala strokes also show a diurnal rate but the cycle is noticeably out of phase with the measured LEMI signal rates. However, since this diurnal cycle disappears when the Vaisala-identified strokes are filtered as described above, this may not be a major contributor to the diurnal LEMI signal rate.

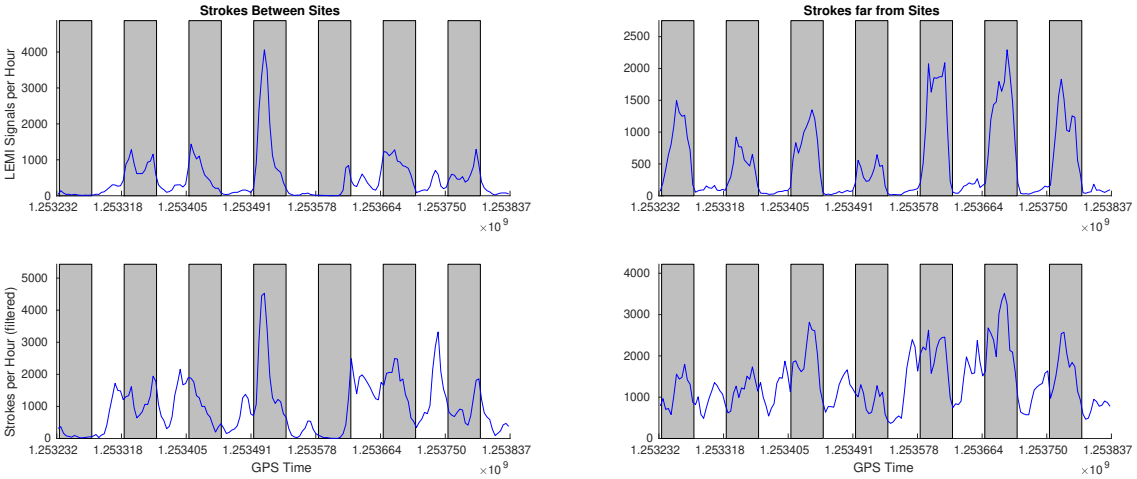

Figure 12: Upper left: Rate of coincident LEMI signals for one week between sites. Shaded regions mark local night at the halfway point between sites. Upper right: Rate of coincident LEMI signals for one week far from sites. Shaded regions mark local night at the halfway point between sites. Coincident signal rate is far more diurnal for distant strokes, peaking during local night. Lower left: Filtered stroke rate of lightning from Vaisala for strokes between sites. Lower right: Filtered stroke rate of lightning from Vaisala for strokes far from sites. Strokes used here are all strokes in the region where strokes coincident with LEMI signals were detected.

4 Gigantic Jets

Since the GLM dataset uses optical measurements from above the clouds, gigantic jets should be more clearly identified in it than cloud to ground strokes. Using the jet observed and methodology described in [14], we can extract the signature of a gigantic jet. Its general morphology (for the loudest event in each group in a flash) consists of a roughly 0.1 s duration pulse with a peak amplitude of order 10^{-14} J. Figure 13 shows the waveform for the jet near Cartagena on November 19, 2018 observed by [14]. The second and third panels show corresponding LEMI signals from this event. At the time of this jet, the Livingston LEMI magnetometers were not connected to the normal bulkheads, so their data feed was sent to a different set of channels (LEMI X channel plugged into L1:PEM-EY_VAULT_SEIS_STS2_Y_DQ and LEMI Y plugged into L1:PEM-EY_VAULT_SEIS_STS2_Z_DQ) (see Livingston alog 43146 [3]). The raw timeseries were filtered with a notch filter at 60 Hz and lowpassed below 55 Hz as this produced the best match to the GLM signal. With LEMI signals so similar to the GLM pixel signal, one can imagine a potential check for jets by matching these two types of time series.

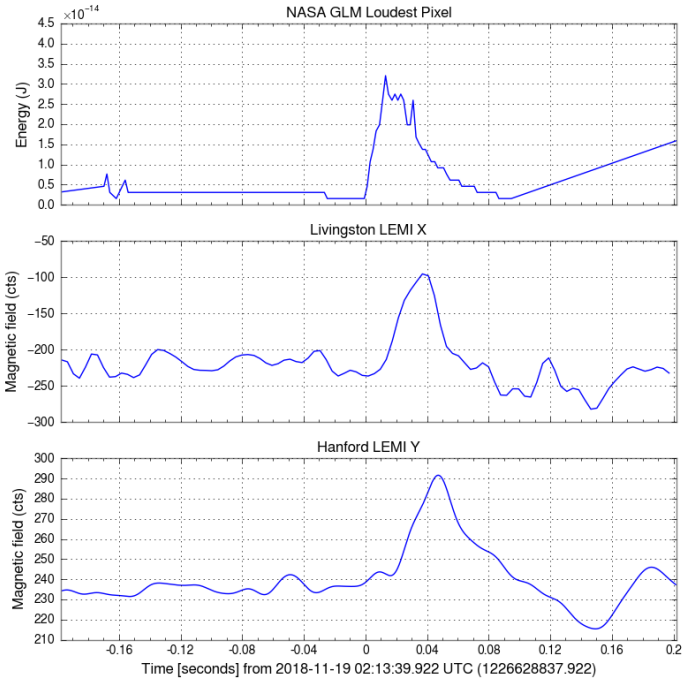

Figure 13: Timeseries of the November 19, 2018 jet near Cartagena. Due to the location of the jet and the orientation of the magnetometers, the two axes presented here show the largest signal due to this jet. Appropriate time offsets for travel time to each site are clear. The presence of such similar signals at both the LEMIs and the GLM data suggests there may be a way to vet for jet signals.

5 Three-Detector Magnetic Coherence with Virgo

So far, this work has only considered magnetic signals coincident between LIGO Hanford and LIGO Livingston in the United States. As the worldwide gravitational wave detector network grows, we need to consider magnetic signals that are coherent on a global scale. We can get an estimate for signals on this global scale by including magnetometers located at Virgo. We then include Omicron triggers from these magnetometers in the pipeline described earlier. Running a coincidence timeslide between magnetic signals that coincided at all three interferometer sites and Vaisala-identified strokes for a 24 hour period gave such a large coincidence spike that the clustering method used before was unnecessary (Figure 14).

Strokes that matched magnetic signals at all three sites are show in Figure 15. Due to the lack of clustering in the coincidence check, there are some miscellaneous signals scattered around that may be purely coincidental. We can see that the majority of signals that match are still found in the Americas, although we now see new sensitivity regions in the northern Mediterranean and eastern Pacific. With Virgo magnetic signals included, there were 8923 total 3-site Omicron triggers, of which 4576 matched Vaisala-identified strokes (51.3%). Of the 45007030 worldwide Vaisala-identified strikes, 4576 matched Omicron triggers (0.0102%).

We also generated plots of the peak current for Vaisala-identified strokes, Omicron SNR for each site, and the peak frequency identified by Omicron. The matched stroke currents (Figure 16) tend towards much higher magnitudes (around ±100 kA) than when looking at signals only matching LIGO Hanford and LIGO Livingston (+10 kA, −40 kA in Figure 7). The matched SNR values for 3-site coincident triggers (Figure 17) tend to favor higher SNR at LIGO Hanford and LIGO Livingston, but the distributions are nearly identical at Virgo. The peaks of the SNR distributions for matched triggers at Hanford and Livingston also are at slightly higher SNR than when looking at only 2-site coincidences (Figure 9). The matched trigger peak frequencies (Figure 18) did not vary much between matched and unmatched signals. At Hanford and Livingston,

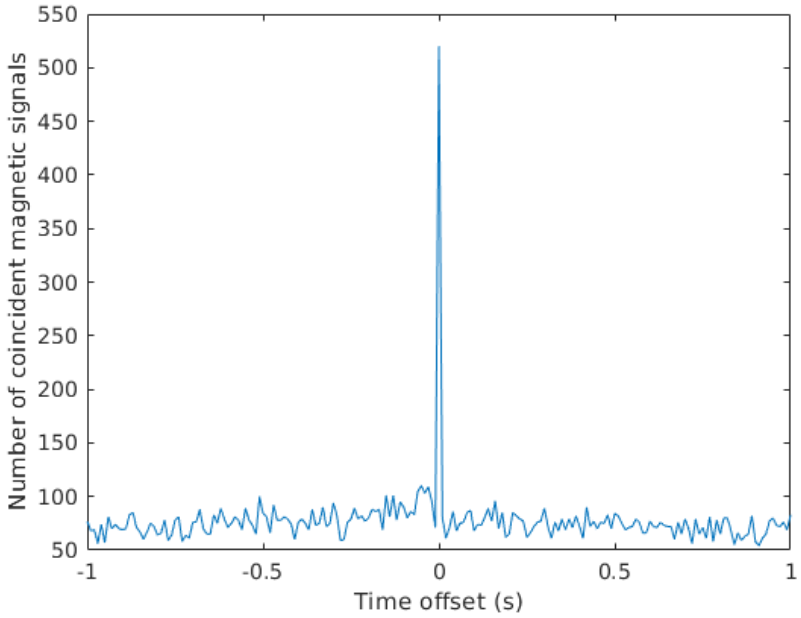

Figure 14: Timeslide of Omicron triggers coincident at Virgo, LHO, and LLO against Vaisala-identified lightning strokes for September 23, 2019. Since the spike in the timeslide exceeded the background by nearly a factor of 5, the clustering method was deemed unnecessary to remove background coincidences.

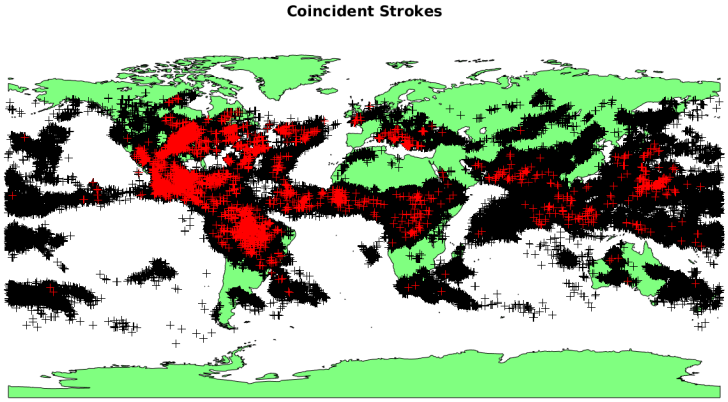

Figure 15: Worldwide lightning strokes from week of September 23, 2019. Red marks are Vaisala-identified strokes that coincided with magnetic signals from LIGO Hanford, LIGO Livingston, and Virgo. This suggests the highest sensitivity to lightning from the Americas.

the matched and unmatched distributions are nearly identical, and at Virgo, the case is nearly the same, though it seems that matched signals slightly tend toward lower frequencies. Also notice that the Virgo distribution does not reach as high frequencies as in the LIGO detectors. This is primarily due to the Virgo magnetometers sampling at a lower rate than the LIGO LEMIs. However, the distribution declines to much lower values before Omicron's cutoff frequency of 630Hz (again limited by a Q-scan's upper limit of 63% of the Nyquist frequency). This suggests some external attenuation to these higher frequencies that we do not have an explanation for.

We also examined the rate of coincident Vaisala-identified strokes coincident with magnetic

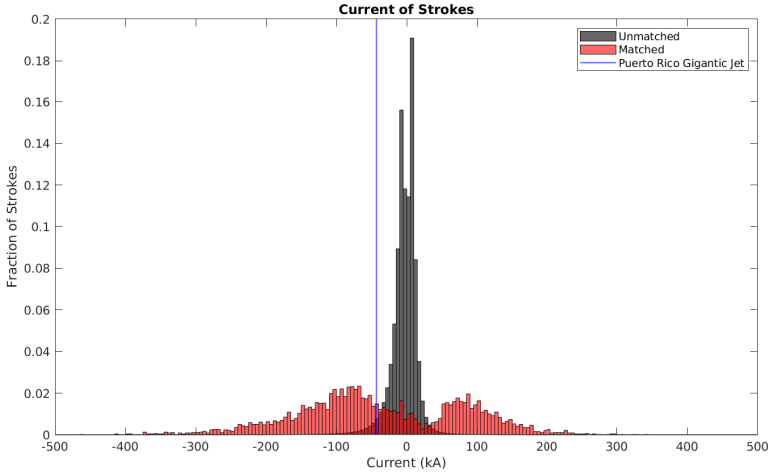

Figure 16: Distribution of peak currents in Vaisala-identified strokes that matched magnetic signals from LIGO Hanford, LIGO Livingston, and Virgo. Unmatched strokes strongly favor low magnitude currents compared to matched strokes which favor higher magnitude currents. Vertical line corresponds to stroke lining up with September 24, 2019 gigantic jet near Puerto Rico. Distributions are normalized to each population.

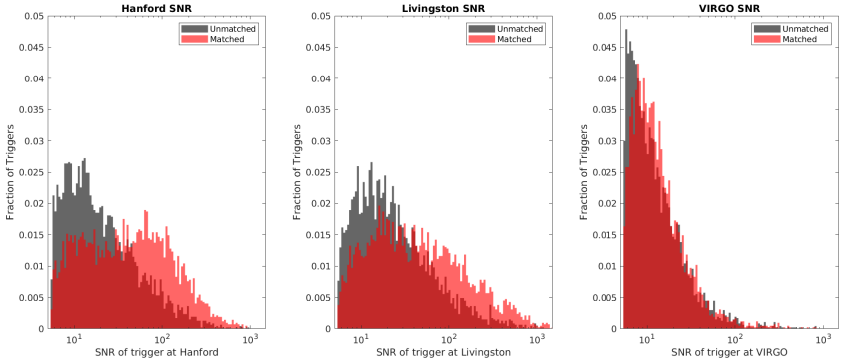

Figure 17: Distribution of Omicron trigger SNR for signals that matched Vaisala-identified strokes. LIGO Hanford and LIGO Livingston triggers that match Vaisala-identified strokes favor higher SNR signals, but there is no noticable difference between matched and unmatched trigger SNR at Virgo. Distributions are normalized to each population.

signals at all three interferometer sites (Figure 19). We still see a diurnal variation in the matched signal rate that lines up with local night in the central United States. This is most likely due to a combination of the increased sensitivity to lightning in the Americas which has a natural diurnal variation in rate as well as the diurnal variation in ionosphere conductivity discussed earlier.

5.1 Axial Omicron Amplitude Coorelation

While trying to find a correlation between the amplitude of a magnetic signal and the distance and current of a Vaisala-identified stroke, we stumbled across an interesting phenomena regarding how the "amplitude" identified by Omicron and the amplitude of that same signal in a time series. They were rarely the same value. Looking a bit deeper, the amplitude Omicron reports is the amplitude of the dominant sine-Gaussian tile in its frequency decomposition [8]. For a broadband signal, this may not be the actual amplitude of the signal.

A true signal amplitude could be obtained by bandpass filtering the signal identified by Omicron around the frequency band Omicron identified. The dominant background is then the 60Hz mains frequency (or 50Hz at Virgo) and harmonics. By notching out these frequencies, all that should remain is the raw magnetic signal detected by Omicron. We can take the maximum amplitude of

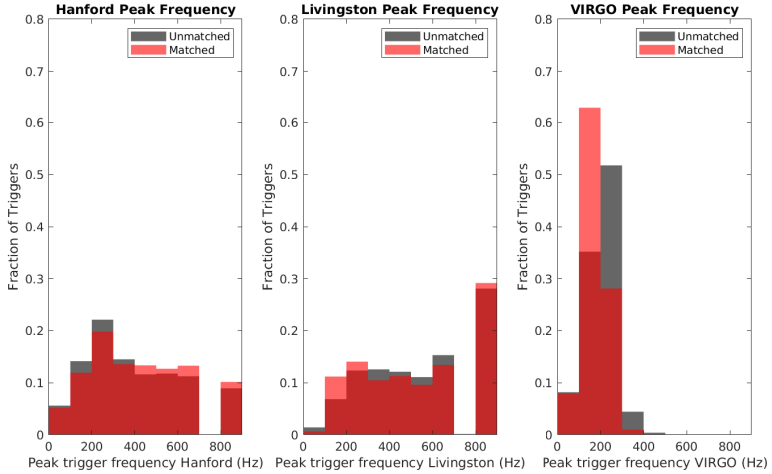

Figure 18: Distribution of peak frequencies identified by Omicron for each site for signals that matched Vaisala-identified strokes. Distributions for the LIGO detectors are somewhat uniform with no real distinction between matched and unmatched signals. The distribution for Virgo triggers is more sharply peaked at lower frequencies. The Virgo magnetometers are sampled at a lower rate, but the distribution still tapers off as it approaches the maximum frequency. Distributions are normalized to each population.

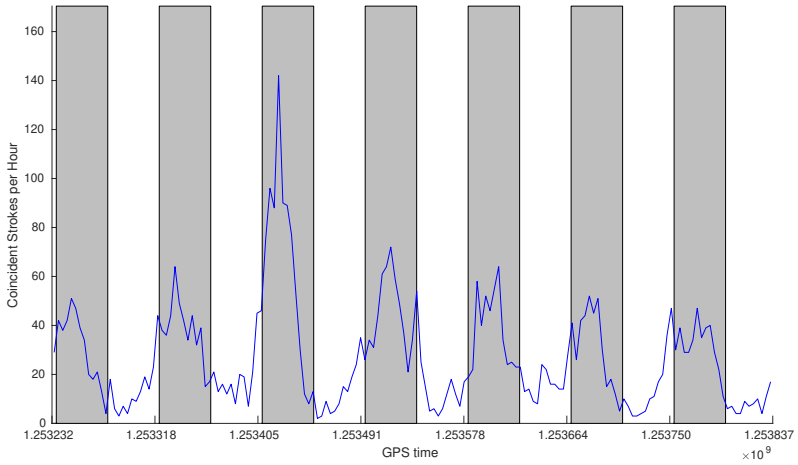

Figure 19: Matched stroke rate for Viasala-identified strokes coincident with magnetic signals at all three interferometer sites. Shaded regions mark local night in the central United States. Even with magnetometers aranged on a global scale, a diurnal variation is still present.

this filtered time series to get a more accurate representation of the magnitude of the magnetic signal. Figure 20 shows plots of the amplitudes identified by Omicron compared to time series amplitudes extracted in this manner. This is run on a random sample of 1000 signals on each channel. Triggers from Hanford and Livingston were taken from the set that was coincident between just Hanford and Livingston, and triggers from Virgo were taken from the set coincident between all three sites. Interestingly, the Omicron amplitudes correlate well for signals on the Hanford Y-axis and the Livingston X-axis, both of which are aligned to best detect signals that occur in the Gulf of Mexico if we assume a lightning stroke to act like a line of current. Triggers coincident between all three sites seen at Virgo showed a fairly constant correlation between Omicron amplitudes and filtered time series amplitudes. This is likely due to the fact that triggers seen at Virgo had a much smaller bandwidth than their LIGO counterparts (Figure 21). This would lead to the amplitude obtained by Omicron being much closer to the time series amplitude instead of only accounting for a small part of a broadband signal.

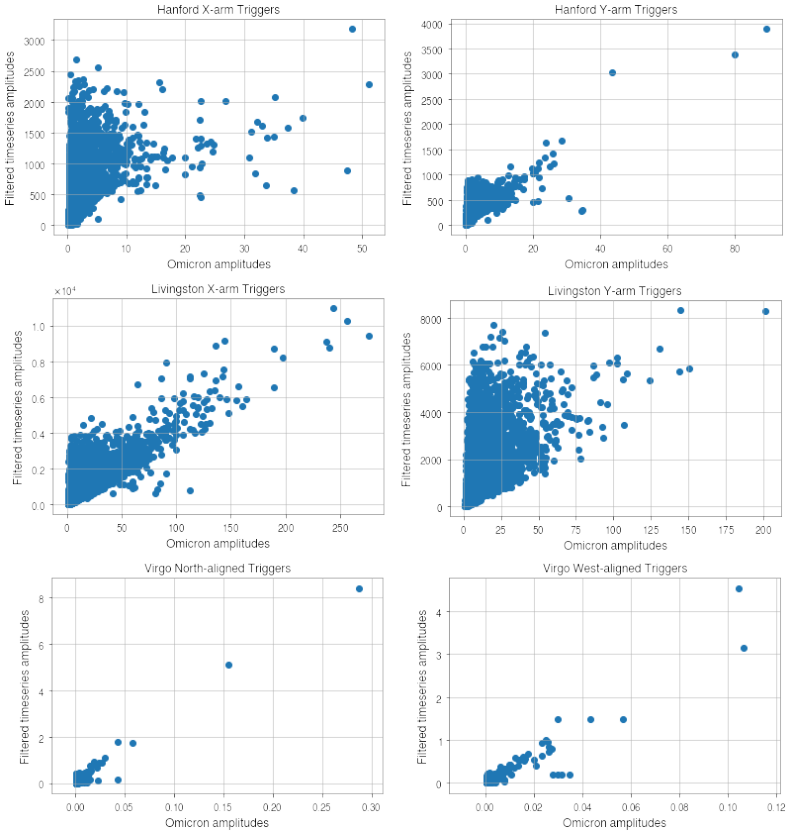

Figure 20: Axis-specific plots of Omicron amplitudes against filtered time series amplitudes. Triggers from Hanford and Livingston were taken from the set that was coincident between just Hanford and Livingston, and triggers from Virgo were taken from the set coincident between all three sites. Certain axes are much more correlated than others. The cause of this is unclear, but

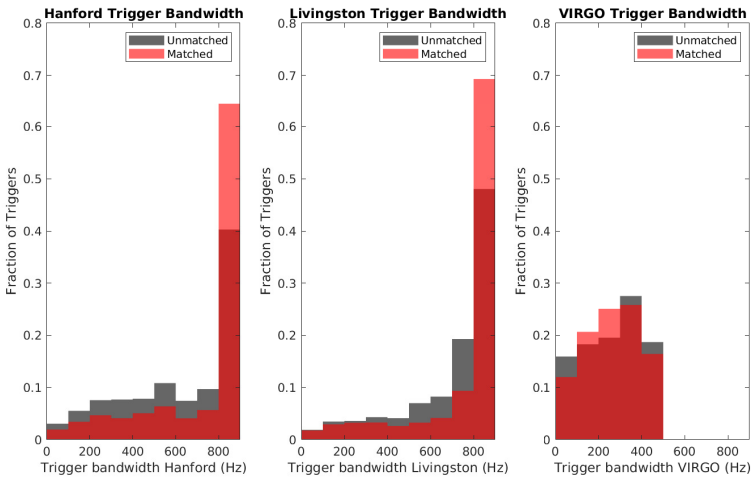

Figure 21: Bandwidth of triggers coincident between all three sites. Signals at the LIGO sites greatly tended toward high bandwith signals unlike signals at Virgo which had much smaller bandwidths. Since the Virgo magnetometers are sampled a much lower frequency than the LIGO LEMIs, the upper limit of around 500Hz is around the Nyquist frequency of the down-sampled signals.

6 Future Work

6.1 Differentiating Lightning from background Omicron Triggers

We also have the need to differentiate a LEMI signal for a real lightning stroke from a signal from some other signal source. Figure 22 (top) shows spectrograms from a series of lighting strokes

near the Livingston detector, and Figure 22 (bottom) shows a corresponding "glitchgram" (time-frequency scatterplot of Omicron triggers colored by SNR) of this magnetometer at the same time.

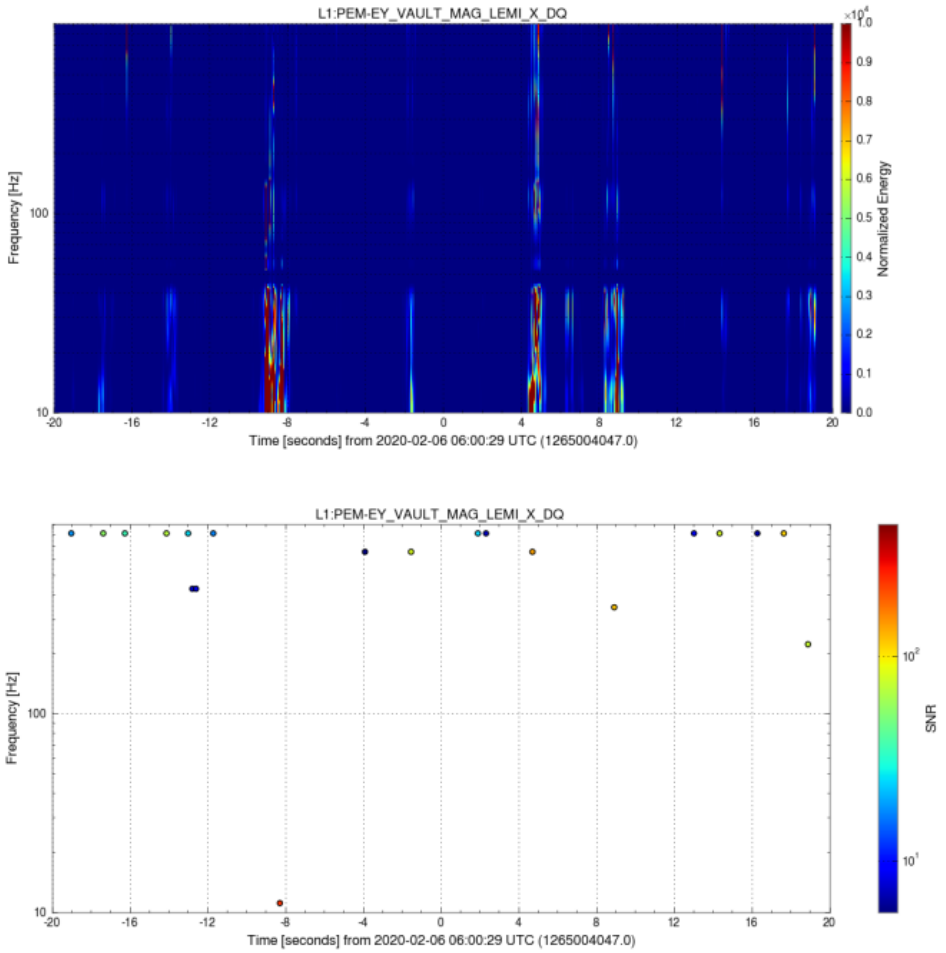

Figure 22: Top: Spectrogram of a series of lightning strokes near the Livingston detector. Bottom: "Glitchgram" of Omicron triggers of this channel during this time. The loudest signals in the spectrogram coincide with Omicron triggers not locked to the maximum allowed value.

Omicron tends to identify the loudest, broadband signals with more middle of the road frequencies, rather than maxed out at the upper limit of the frequency search range. Notice the 4 triggers on Figure 22 with frequencies below 500 Hz. These line up the best with the broadband signals shown in the spectrogram of Figure 22.

6.1.1 Analytic Description

We also have a need to easily identify potential strokes without requiring an external source such as the GLD360 or GLM datasets. Since a lightning stroke is essentially a line of current, we can model its magnetic field as that from a line of current, which goes as $1/r$. With the time of arrival difference between the two sites and the relative amplitudes of the signals at each site, we can estimate the distance to the source.

For signals traveling along the surface of the planet (as we expect of these magnetic signals), we can parameterize the magnetic field strength at each site in terms of the distance from the stroke to only one stroke. Since a direct path for the signal to take along a sphere is a great circle, the distance from the source to one site r_1 and the distance from the source to the other site r_2 can be related by the effective distance due to the time delay $\Delta r = c\Delta t$ where c is the speed of light and Δt is the time delay. Choosing $\Delta t = t_2 - t_1$, we can express the magnetic field strengths at each site as:

$$B_1 = \frac{\alpha_1}{r_1} \qquad\qquad B_2 = \frac{\alpha_2}{r_2 + c\Delta t}$$

where α_i is a scalar constant dependent on the current of the stroke. For both signals to be produced from the same stroke, we must have $\alpha_1 = \alpha_2$, allowing us to get the relation:

$$r_1 = \frac{B_2 \; c(t_2 - t_1)}{B_1 - B_2}$$

For a pair of coincident LEMI signals to be real, it is logical that this value is both greater than 0 and less than some maximum distance that the LEMIs are not sensitive to. From the analysis of the GLD360 data, we observed a maximum distance of 7277 km and 8629 km from Livingston and Hanford, respectively.

We enforce limits on the distance of a stroke from Livingston and Hanford as well as requirements that both estimated distances can actually exist simultaneously: the sum of the distances must be greater than or equal to the distance between the sites, and the difference between the distances cannot exceed the distance between the sites. We also require that the estimated distances to each site be physically possible at the same time (eg. we cannot have a signal originate from a source that is simultaneously 1km from Hanford and 1km from Livingston). Unfortunately, with only two locations, we cannot fully localize the source of a given signal. Currently, triggers selected by this method only match Vaisala-identified strokes with about 60% accuracy.

6.2 Effect on Gravitational Wave Readout

Currently, coupling functions from the LEMI magnetometers to the main gravitational wave readout channel are being measured at Hanford. These are frequency-space functions that predict the potential impact of a signal in an auxiliary channel on DARM. Once these functions are properly measured, we can use them to predict the impact of these signals on DARM as the detectors are improved and sensitivity increases. This will give an estimate on potential false alarm rates for these sorts of coincident signals which are important for long-duration stochastic searches.

Appendices

A GLM Time Offset

The GLM data is recorded in Terrestrial Time (TT), so to compare it to LIGO data on GPS time, we need to convert this to UTC. Additionally, the TT used by the GLM is recorded in seconds from 12:00pm, January 1, 2000. This reference time has a slight offset from UTC of 32.184 s, so the theoretical exact offset of the two time systems is 630763143.816 s. Using this time offset to find the known jet on September 24 produced no result, so we still needed something else.

To find the true offset, we compared the GLM data to the GLD360 data. Starting from the pre-established time offset, we ran a timeslide between the two data sets for signals occuring at the same place and same time in the latitude range $(0, 20)$ and longitude range $(-110, -70)$ to save on computation time. This comparison produced more than one spike in the timeslide. The spikes that were observed gave additional time offsets of either +74.18 s or +99.183 s. To resolve this, we used an observed jet signal from van der Velde et al [14] recorded near Cartanega on November 19, 2018 as another check. The paper looks at the time series of the loudest "event" of each "group" in a "flash" (basically tracking the loudest pixel of each cluster from frame to frame) to get a waveform of sorts. Finding the signal shown in the paper gives an offset of +74.18 s, matching one of the offsets from the previous timeslide.

References

[1] Michael W. Coughlin et al. "Measurement and subtraction of Schumann resonances at gravitational-wave interferometers". In: *Phys. Rev. D* 97 (10 May 2018), p. 102007. DOI: 10.1103/PhysRevD.97.102007. URL: https://link.aps.org/doi/10.1103/PhysRevD.97.102007.

[2] Nicholas Demetriades, Martin Murphy, and J.A. Cramer. "Validation of Vaisala's Global Lightning Dataset (GLD360) over the continental United States". In: (Jan. 2010).

[3] Anamaria Effler. *LEMI magnetometer situation since O2 - all back to nominal*. 2019. URL: https://alog.ligo-la.caltech.edu/aLOG/index.php?callRep=43146.

[4] GOES-R Algorithm Working Group GOES-R Algorithm Working Group and GOES-R Series Program. *NOAA GOES-R Series Geostationary Lightning Mapper (GLM) Level 2 Lightning Detection: Events, Groups, and Flashes*. 2018. DOI: 10.7289/V5KH0KK6. URL: https://www.ncei.noaa.gov/metadata/geoportal/rest/metadata/item/gov.noaa.ncdc%3AC01527/html.

[5] Kamiel Janssens. *Globally coherent magnetic fields at high frequencies*. LIGO Document Control Center. 2020. URL: https://dcc.ligo.org/LIGO-G2001492.

[6] K. Naccarato et al. "VALIDATION OF THE NEW GLD 360 DATASET IN BRAZIL : FIRST RESULTS 1". In: 2010.

[7] Tony Philips. *Close Encounter with a Gigantic Jet*. spaceweather.com. 2019.

[8] Florent Robinet et al. *Omicron: a tool to characterize transient noise in gravitational-wave detectors*. 2020. arXiv: 2007.11374 [astro-ph.IM].

[9] Scott D. Rudlosky et al. "Initial Geostationary Lightning Mapper Observations". In: *Geophysical Research Letters* 46.2 (2019), pp. 1097–1104. DOI: 10.1029/2018GL081052. eprint: https://agupubs.onlinelibrary.wiley.com/doi/pdf/10.1029/2018GL081052. URL: https://agupubs.onlinelibrary.wiley.com/doi/abs/10.1029/2018GL081052.

[10] M. Saba et al. "High-speed video observations of positive lightning flashes to ground". In: *Journal of Geophysical Research* 115 (Dec. 2010). DOI: 10.1029/2010JD014330.

[11] R. K. Said, M. B. Cohen, and U. S. Inan. "Highly intense lightning over the oceans: Estimated peak currents from global GLD360 observations". In: *Journal of Geophysical Research: Atmospheres* 118.13 (2013), pp. 6905–6915. DOI: 10.1002/jgrd.50508. eprint: https://agupubs.onlinelibrary.wiley.com/doi/pdf/10.1002/jgrd.50508. URL: https://agupubs.onlinelibrary.wiley.com/doi/abs/10.1002/jgrd.50508.

[12] R. K. Said, U. S. Inan, and K. L. Cummins. "Long-range lightning geolocation using a VLF radio atmospheric waveform bank". In: *Journal of Geophysical Research: Atmospheres* 115.D23 (2010). DOI: 10.1029/2010JD013863. eprint: https://agupubs.onlinelibrary.wiley.com/doi/pdf/10.1029/2010JD013863. URL: https://agupubs.onlinelibrary.wiley.com/doi/abs/10.1029/2010JD013863.

[13] Fernando Simões et al. "A Review of Low Frequency Electromagnetic Wave Phenomena Related to Tropospheric-Ionospheric Coupling Mechanisms". In: *Space Science Reviews* 168.1 (June 2012), pp. 551–593. ISSN: 1572-9672. DOI: 10.1007/s11214-011-9854-0. URL: https://doi.org/10.1007/s11214-011-9854-0.

[14] Oscar A. van der Velde et al. "Gigantic jet discharges evolve stepwise through the middle atmosphere". In: *Nature Communications* 10.1 (Sept. 2019), p. 4350. ISSN: 2041-1723. DOI: 10.1038/s41467-019-12261-y. URL: https://doi.org/10.1038/s41467-019-12261-y.